Size effect of Silver Nanoparticles on the Luminescence Properties of Nearby Cardon Dots

M.Sc. Thesis

By Bhaswati Sarkar



DISCIPLINE OF CHEMISTRY INDIAN INSTITUTE OF TECHNOLOGY INDORE

June, 2016

Size effect of Silver Nanoparticles on the Luminescence Properties of Nearby Cardon Dots

A THESIS

Submitted in partial fulfillment of the requirements for the award of the degree of

Master of Science

by

BHASWATI SARKAR



DISCIPLINE OF CHEMISTRY INDIAN INSTITUTE OF TECHNOLOGY INDORE

June, 2016

Acknowledgements

I would like to convey my humble gratitude to **Dr. Tushar Kanti Mukherjee**, (Associate Professor, Discipline of Chemistry, IIT Indore, Indore) for giving me an opportunity to work in the field of my interest with his research group. I never would have been able to get this far without his invaluable suggestions and productive criticism. I am obliged for his valuable suggestions and discussions which helped me in gaining not only a better understanding of the subject and critical analysis of the results but also to develop enthusiasm for further scientific research. Without his assistance and support it would have really been difficult for me to achieve my goals. So I am indebted to him for his support, motivation and better understanding.

I would also like to extend my gratitude to **Dr. Apurba K. Das**, and **Dr. Srivathsan Vasudevan** for their valuable suggestions and guidance.

I am extremely indebted to my lab-mates who provided me with a great place and healthy environment to work. I would like to especially thank Dr. Vijaykant Khorwal, Mr. Surajit Chatterjee, Miss Roopali Prajapati, Mr. Arpan Bhattacharya, Miss Jamuna Vaishnav, and Mr. Somnath Das for their valuable suggestion and cooperation. I would be very thankful to all the faculty members of Discipline of Chemistry for their motivational inspiration.

I would like to thank Discipline of Chemistry, IIT Indore for facility and infrastructure. I am also thankful to SIC, IIT Indore and its member for their technical help and support.

Last but not the least I would like to extend my heartfelt gratitude, love and regards to my ever loving parents for their endless encouragement, support and faith in me. Without their blessings and care, I would never have reached to a platform where I stand now.

DEDICATED TO MY LOVING PARENTS

Abstract

To know the effect of localized surface plasmon resonance (LSPR), on the luminescence of the nearby fluorophore shell, silver nanoparticles (Ag NPs) and a core-shell nanoconjugate Ag@SiO₂NPs have been synthesized and interaction with carbon dots (CDs) is studied by fluorescence spectroscopy and time-correlated single photon counting (TCSPC). In the present study, we have demonstrated the excitation energy transfer (EET) from carbon dots (CDs) to the uncoated silver nanoparticles and SiO₂ coated silver nanoparticles (Ag@SiO₂NPs). Spectral overlap between the emission spectrum of CDs and localized surface plasmon resonance of Ag NPs results in PL quenching of CDs. A more significant spectral overlap between the emission spectrum of CDs and localized surface plasmon resonance of Ag@SiO2 NPs result in drastic increase PL quenching. In addition, the PL lifetime of CDs is shortened more when the coating was done the three different size bare Ag NPs. The origin of this PL quenching has been rationalized on the basis of increased nonradiative decay rate due to excitation energy transfer from CDs to Ag NPs surface. The observed energy-transfer efficiency correlates well with the nanometal surface energy transfer theory with 1/d⁴ distance dependence rather than conventional Förster resonance energy transfer theory. Finally, the energy-transfer efficiency values obtained from experiment have been used to calculate the distance between CDs and surface of uncoated and SiO₂ coated Ag NPs.

Table of Content

Contents		Page No.
	Glossary of Acronyms	ix
	Glossary of Mathematical	
	terms	X
	List of Figures	xi-xii
	List of Tables	Xiii
Chapter 1.		
Introduction		1-4
Chapter 2.		
Experimental Section		5-8
	2.1 Materials	5
	2.2. Synthesis of Carbon dot	5
	2.3.Synthesis of Silver	
	nanoparticle (Ag NPs)	6
	2.4. Synthesis of Core-Shell	6-7
	Ag@SiO ₂ nanoparticles	0-7
	2.5. Instrumentation	7-8
Chapter 3.		
Results and discussion		
	3.1.Characterization of Ag	9-13
	NPs and Ag@SiO ₂ NPs	9-13
	3.2. Characterization of	13-14
	carbon dots	13-14
	3.3.Interaction between C-	14-15
	dot and Ag NPs	1110

3.4. Steady –State PL	
Quenching of CDs in the	15-18
presence of Ag NPs and	13-16
Ag@SiO ₂ NPs.	
3.5.Time-Resolved PL	
quenching of CDs in the	18-23
presence of ANPs	
3.6. Mechanism of EET	23-25
from CDs to Ag NPs	23-23
4.1. Conclusions	26
4.2. Scope for Future work	26
References	27-34
	Quenching of CDs in the presence of Ag NPs and Ag@SiO ₂ NPs. 3.5.Time-Resolved PL quenching of CDs in the presence of ANPs 3.6. Mechanism of EET from CDs to Ag NPs 4.1. Conclusions 4.2. Scope for Future work

Glossary of Acronyms

Ag NPs Silver nanoparticles

Ag@SiO₂ NPs SiO₂ coated silver nanoparticles

CDs Carbon dot

EET Excitation energy transfer

FRET Froster resonance energy transfer

SET Surface energy transfer

TCSPC Time correlated single photon counting

UV Ultraviolet

Vis Visible

IR Infrared

IRF Instrument response function

Glossary of Mathematical terms

M Molar

 λ_{em} Emission wavelength

 λ_{ex} Excitation wavelength

 τ_i Lifetime of i^{th} component

 χ^2 Reduced chi-square

 a_i Amplitude of the i^{th} component in a multiexponential decay

 k_r Radiative decay rate

 k_{nr} Non-radiative decay rate

 R_0 Förster distance

d₀ Separation distance between donor and acceptor at which

the energy-transfer efficiency is 50%

 Φ_D Fluorescence quantum yield of donor

 Φ_{Eff} Efficiency

 Φ_{Et} Energy transfer efficiency

Å Angstrom

 ε Molar extinction coefficient

Nm Nanometer

 GO_D The angular frequency of the donor electronic

Transition.

GO_F Fermi frequency

K_F Fermi wave

vector of the metal

List of Figures

Content		Page
		No.
Figure 1.	Synthetic strategy of Carbon Dots (CDs) using	5
	citric acid and ethylenediamine.	
Figure 2.	Synthetic strategy of silver nanoparticles using	6
	citric acid by the well-known Lee and Meisels	
	method with slight modification.	
Figure 3.	Synthesis of Ag@SiO ₂ NPs.	7
Figure 4.	Size distribution histogram of small (A), medium	10
	(B) and large (C) Ag NPs from DLS	
	measurements.	
Figure 5.	Size distribution histogram of small (A), Medium	11
	(B) and large (C) Ag@SiO ₂ NPs from DLS	
	measurements.	
F: (Channelly LCDD of analy (A) and have (D) and	10
Figure 6.	Change in LSPR of small (A), medium (B) and	12
	large (C) silver nanoparticles when coated with	
	silica layer	
Figure 7.	FTIR spectrum of synthesized CDs.	13

Absorbance spectrum (black line) and the Figure 8. 14 normalized PL ($\lambda_{ex} = 493$ nm) spectrum (green line) of CDs. Figure 9. Absorption spectrum of CDs in the presence of 15 (A) small, (B) medium, (C) large Ag NPs at their different concentrations. Figure 10. PL spectra of C-dot in presence of (A) Ag NPs and 16 (B) $Ag@SiO_2$ NPs. Figure 11. Normalized PL spectrum of CDs (black line) 17 overlapped with the LSPR of uncoated (red line) and coated (blue line) (A) small (B) and (C) large silver nanoparticles. PL decay traces ($\lambda_{ex} = 405$ nm) of CDs in the Figure 12. 18 presence of (A) uncoated Ag NPs and (B) Sicoated Ag NPs at different diameter. Figure 13. Correlation between experimentally obtained EET 25 efficiencies for the CDs-Ag NPs system with the theoretical curves generated from NSET (red line).

List of Table

Content		Page
		No.
Table 1	PL Decay parameters of CDs, CDs with	19
	uncoated and coated small Ag NPs.	
Table 2	PL Decay parameters of CDs, CDs with	20
	uncoated and coated medium Ag NPs.	
Table 3	PL Decay parameters of CDs, CDs with	20
	uncoated and coated large Ag NPs.	
Table 4	Estimated Quantum Yields, Average Lifetime,	21
	Radiative Rates, Nonradiative Rates, Energy	
	Transfer Rates, and Efficiency of Energy	
	Transfer of CDs in the absence and presence of	
	uncoated and coated small Ag NPs.	
Table 5	Estimated Quantum Yields, Average Lifetime,	22
	Radiative Rates, Nonradiative Rates, Energy	
	Transfer Rates, and Efficiency of Energy	
	Transfer of CDs in the absence and presence of	
	uncoated and coated medium Ag NPs.	
Table 6	Estimated Quantum Yields, Average Lifetime,	22
	Radiative Rates, Nonradiative Rates, Energy	
	Transfer Rates, and Efficiency of Energy	
	Transfer of CDs in the absence and presence of	
	uncoated and coated large Ag NPs.	

Chapter 1.

Introduction

Semiconductor nanoparticles have attracted growing attention for widespread use in bioimaging, [1] light emitting, [2] solar cells, [3, 4] photocatalyst, [5] optical spectroscopy-based immunoassays, [6] and data storage. [7] Excitation energy transfer in nanoscale donor-acceptor system has a large-scale implementation in the sensor, photovoltaic devices, light emittors, and other optoelectronics. [8-12] Nonradiative energy transfer from a photoexcited donor to an acceptor via dipole-dipole interactions is well-known as Förster resonance energy transfer (FRET). FRET is a through-space distance dependent Interaction from photoexcited donor to an acceptor without emission of a photon. [13-18]

However, currently, metal and semiconductor nanoparticles (NPs) based donor-acceptor nanocomposite systems have achieved significant attention due to their extraordinary diverged optoelectronic properties, which allow easy tuning of energy-transfer efficiency. [19-24] Novel metals such as silver (Ag), gold (Au), and copper (Cu) show localized surface plasmon resonance (LSPR) in the visible region of the electromagnetic spectrum. [25-26] This occurrence of the metal surface has been greatly applied in surface-enhanced Raman scattering, [27-28] near-field scanning probe microscopy, [29-30] and fluorescence enhancement at the metal surface. [31-36] The effect of metal nanocomposite the PL quantum yield of nearby fluorophore is very complex. It is controlled by various parameters such as size and shape of the metal nanostructures, an orientation of dipole on the metal nanostructure, the distance between fluorophore and metal nanostructure, and spectral overlap. Metal nanoparticles can either enhance or quench the PL quantum yield of the nearby fluorophores. Wu et al. reported meditating metal coenhanced fluorescence and SERS around gold nano aggregates in nanosphere as a bifunctional biosensor for multiple DNA targets. [37] They have also reported a novel Ag core and

upconversion nanocrystal shell based nanocomposite Ag@SiO₂@Lu₂O₃:Gd/Yb/Er metal-enhanced upconversion for luminescence literature^[1]. The excitation energy transfer (EET) from silicon quantum dots (Si QDs) to silver nanoparticles (Ag NPs) and its modulation in the presence of cetyltrimethylammonium bromide (CTAB) surfactant is reported by Prajapati et al. [38] Several other research groups have demonstrated the influence of metal nanostructure on the fluorescence of nearby fluorophore. For instance, SiO₂-coated metal nanostructure, Ag nanoprisms, and Au NP's surface enhances the fluorescence of CdSe/ZnS QDs, and amine-functionalized pyrene chromophores (Py-CH₂NH₂) respectively. [39-41]

Quenching of fluorescence of various fluorophore by metal nanoparticles is also reported in various literature. For example, Raghavendra *et al.* have shown fluorescence quenching of iodinated 4-aryloxymethyl coumarin dyes with the addition of silver nanoparticles. [42] Chance *et al.* has exhibited that fluorescence quenching of excited donor in the presence of metal NPs. [43] Later, it is extended by Persson and Lang by using a Fermi Golden Rule. [44] This dipole-to-metal surface excitation energy transfer is known as nanometal surface energy transfer (NSET). The origin behind this fluorescence quenching in the presence of metal nanoparticles is due to modulation of either radiative [45] or nonradiative [23, 46, 47] decay rate or both. [48] A fundamental difference between FRET and NSET is that for the later process spectral overlap between donor emission and the acceptor absorption is not the essential criteria. Jennings *et al.* have demonstrated fluorescence of dye-quenched by Au nanoparticles at a donor-acceptor separation distance d = 1.5 nm, which is a lack of SPR. [46]

Here they have revealed that a 1/d⁴ distance-dependent quenching mechanism due to nonradiative energy transfer to the metal surface, while radiative rate remains constant. On the other hand, Li *et al.* have demonstrated both the effect of metal nanoparticles size and the degree of spectral overlap on the energy-transfer process between CdSe/ZnS QDs

and Au NPs.^[49] It has been noted that 3 nm sized Au NPs with negligible LSPR, the quenching mechanism of the PL of QDs is 1/d⁴ distance dependence which leads to NSET, while 15 and 80 nm sized Au NPs with strong LSPR band that significantly overlaps with the PL band of the QDs quenching mechanism is 1/d⁶ distance dependence, which is dominated by the dipole–dipole interaction according to FRET.

However, core-shell based inorganic based QDs have several significant disadvantages in biomedical application due to their bigger size and cytotoxicity. [50-51] Hence to resolve these side effects, of these type inorganic based QDs in bio imaging, a carbon-based fluorescent nanomaterial particularly CDs have been attracted more attention of researchers as a most promising candidate for biomedical imaging applications as a consequence of their low cytotoxicity, smaller size, and easy surface functionalization with comparable PL properties to core–shell inorganic based QDs. CDs have numerous advantages over traditional semiconductor quantum dots and organic dyes. CDs are becoming an extraordinary nanomaterial because of its aqueous solubility, low cytotoxicity, biocompatibility and resistance to photobleaching. Also, CDs can be synthesized easily from several natural sources like candle soot, carbohydrate, polyhydric alcohol, polyhydric acid, orange juice, strawberry juice, cucumber juice, banana juice. [1, 44, 52-55] The main aspect of carbon dots is the development of fluorescence imaging agents for various biomedical purposes. Thus modulation of fluorescence emissions of CDs is one of the exciting goals to worldwide researchers. [56]

Among the various systems described above, the size effect of Ag NPs on luminescence properties of nearby CDs is not yet explored. Hence, in this report, three different sized silver nanoparticles have been synthesized. To increase the donor-acceptor interaction distance, a coating was done on the three different size Ag NP's core. Here we have investigated the distance-dependent interaction of uncoated and coated Ag NPs with CDs. We have shown that spectral overlap between the

luminescence spectra of CDs and LSPR of Ag NPs increases with increase in the size of Ag NPs and nonradiative EET increases following NSET theory rather than conventional FRET theory.

Chapter 2.

Experimental Section

2.1 Materials

Silver Nitrate (\geq 99%), Tri-sodium Citrate dihydrate (Na₃C₆H₅O₇.2H₂O), tetraethylorthosilicate (TEOS), Ethanol, Ammonium Hydroxide, Ethylenediamine (EDA, Z 99.5%), isopropyl alcohol (99 %) were purchased from Merck (Germany). Milli-Q water was used wherever required and obtained using a Millipore water purifier system (Milli-Q Integral).

2.2 Synthesis of carbon dots (CDs)

Carbon-dots were synthesized according to the previously reported method (Scheme 1). ^[54] In brief; citric acid (1.015 g) and ethylenediamine (335 mL) were dissolved in Milli-Q water (10 mL) and sonicated for 5 min. Then the solution was transferred to a Teflon-coated stainless steel autoclave (25 mL) and heated at 200 °C for 5 h. Subsequently, the reactor was cooled to room temperature and the solution was dialyzed (MWCO 3.5 kDa) for 48 h. The water for dialysis was changed after every 6 h. Finally, a black brown transparent c-dot solution was obtained.

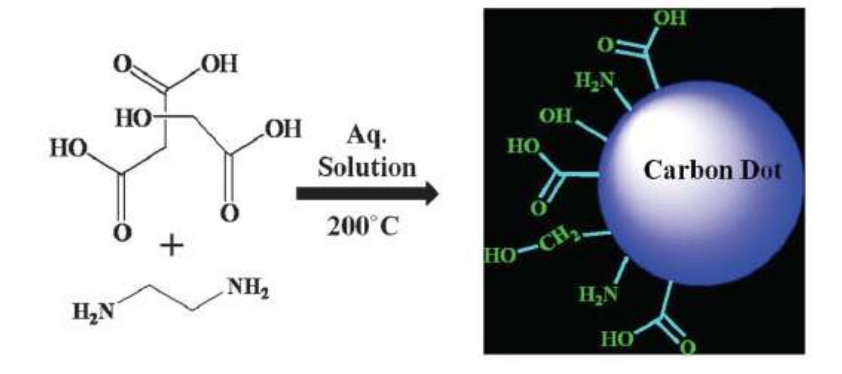


Figure 1.Synthetic strategy of Carbon Dots (CDs) using citric acid and ethylenediamine.

2.3. Synthesis of silver nanoparticles

Three different diameters silver NPs were prepared by the well-known Lee and Meisels method with slight modification. [38, 57] Three solutions of AgNO₃ ($\sim 1.0 \times 10^{-3}$ M, 100 mL) in deionized water were heated until boiling. Then, 16 mL of (1%, 0.875%, and 0.75%) tri-sodium citrate solution were added drop-wise to the boiling silver nitrate solutions accompanied by vigorous stirring. The color of the solutions slowly turned into grayish yellow, indicating the reduction of the Ag⁺ ions. The heating was continued for an additional 15 min. Finally, three green-gray silver colloid were obtained. Then, the three solutions were removed from the heating element and stirred until cooled to room temperature. The final concentration of the as-synthesized three different sized was estimated using the molar extinction coefficient at maximum LSPR wavelengths $\epsilon_{415} = 416 \times 10^8$, $\epsilon_{425} = 618 \times 10^8$ and $\epsilon_{435} = 618 \times 10^8$ M⁻¹ cm⁻¹ and found to be ~ 23.8 , 16 and 13 pM respectively. [58] The diameter of the obtained Ag NPs was characterized by dynamic light scattering method (DLS).

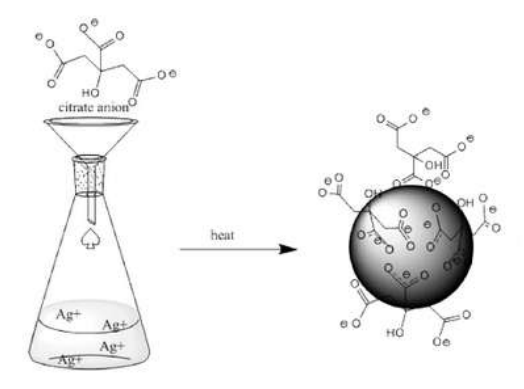


Figure. 2. Synthetic strategy of silver nanoparticles using citric acid by the well-known Lee and Meisels method with slight modification.

2.4 Preparation of Core-Shell Ag@SiO₂ NPs.

Core-shell Ag@SiO₂ NPs was obtained according to the literature^[59] with slight modification. Briefly, 1 mL of Ag colloid solution was mixed with 12.5 mL of isopropyl alcohol and 1.25 mL of deionized

water under vigorous stirring. After the addition of 0.2 mL of 30% $NH_3 \cdot H_2O$, 5 μL of a TEOS solution with a concentration of 20% was immediately added into the mixed reactants. The reaction was carried out under agitation for 30 min at room temperature (RT), and then the products were aged without stirring at 4°C overnight. The silica-coated were redispersed in water suspension was washed three times with a water and ethanol mixture (5:4) and centrifuged at 6000 rpm for 20 min. Finally, the core_shell $Ag@SiO_2$ NPs were dispersed in water .Thus, three different sized $Ag@SiO_2$ NPs were synthesized and the diameter of the obtained $Ag@SiO_2$ NPs was characterized by dynamic light scattering method (DLS).

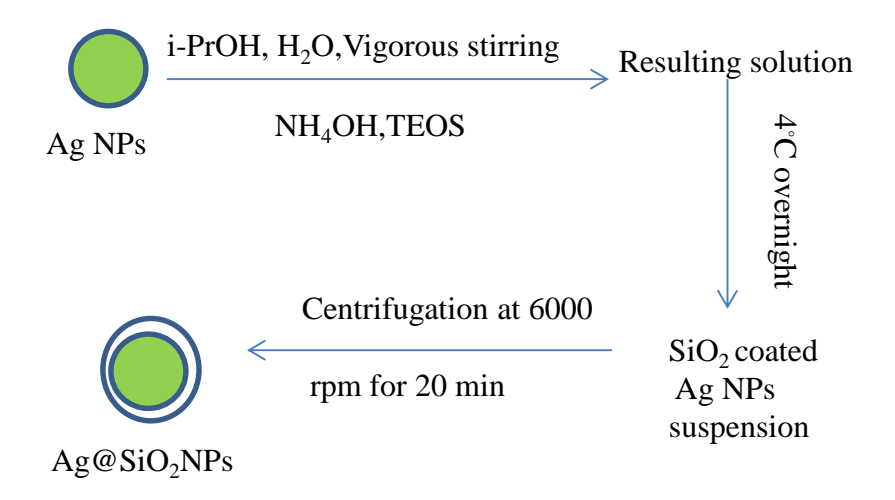


Figure 3. Synthesis scheme of Ag@SiO₂ NPs.

2.5 Instrumentation

Absorption spectra were recorded using a Varian UV-vis spectrophotometer (Carry 100 Bio) in a quartz cuvette (10×10 mm). PL spectra were recorded using Fluoromax-4 spectrofluorometer (HORIBA Jobin Yvon, model FM-100) with excitation and emission slit width at 2 nm. DLS experiment was performed on a particle size analyzer (NanoPlus-3 model). All of the samples for DLS measurements were prepared in milli-Q water and filtered through a 0.22 μ m syringe filter

(Whatman). An HORIBA JobinYvon picosecond time-correlated single photon counting (TCSPC) spectrometer (model Fluorocube-01-NL) was used for recording PL decays. The samples were excited at 405 nm by a picoseconds diode laser (model Pico Brite-375L). The emission polarizer at a magic angle of 54.7° by a photomultiplier tube (TBX-07C) was used to collect the PL decays. The instrument response function (IRF, fwhm \sim 140 ps) was recorded using a dilute scattering solution. The IBH DAS 6.0 software was used to analyze the PL decays by the iterative reconvolution method, and the goodness of the fit was judged by reduced χ -square (χ^2) value. All of the decays were fitted with a three-exponential function

$$F(t) = \sum_{i=1}^{3} a_i \exp(-t/\tau_i)$$
 (1)

Where F(t) denotes normalized PL decay and a_1 , a_2 , and a_3 are the normalized amplitudes of decay components τ_1 , τ_2 , and τ_3 respectively. The average lifetime was obtained from the equation

$$\langle \tau \rangle = \sum_{i=1}^{3} a_i \tau_i$$
 (2)

Chapter 3.

Results and Discussion

3.1 Characterizations of Ag NPs, Ag@SiO₂ NPs

To estimate the mean hydrodynamic diameter of these Ag NPs, DLS measurements were performed for small, medium and large Ag NPs. Figure 4 (A) Shows the size distribution histogram small Ag NPs determined from DLS measurements. The diameter varies from 38 to 41 nm with a mean diameter of 39.91 nm. Figure 4 (B) Shows the size distribution histogram of medium Ag NPs determined from DLS measurements. The diameter varies from 52 to 54 nm with a mean diameter of 53 nm and Figure 4. (C) Shows the size distribution histogram of large Ag NPs determined from DLS measurements. The diameter varies from 60 to 63 nm with a mean diameter of 62 nm. Large Ag NPs from DLS measurements.

To estimate the mean hydrodynamic diameter of the Ag@SiO₂ NPs, DLS measurements were performed for small, medium and large size SiO₂ coated silver nanoparticles. Figure 5 (A) Shows the size distribution histogram of small Ag@SiO₂ NPs determined from DLS measurements. The diameter varies from 80 to 200 nm with a mean diameter of 119 nm. Figure 5 (B) shows the size distribution histogram of medium Ag@SiO₂ NPs determined from DLS measurements. The diameter varies from 85 to 197 nm with a mean diameter of 132 nm. Figure 5 (c) shows the size distribution histogram of large Ag@SiO₂ NPs determined from DLS measurements. The diameter varies from 60 to 350 nm with a mean diameter of 144 nm.

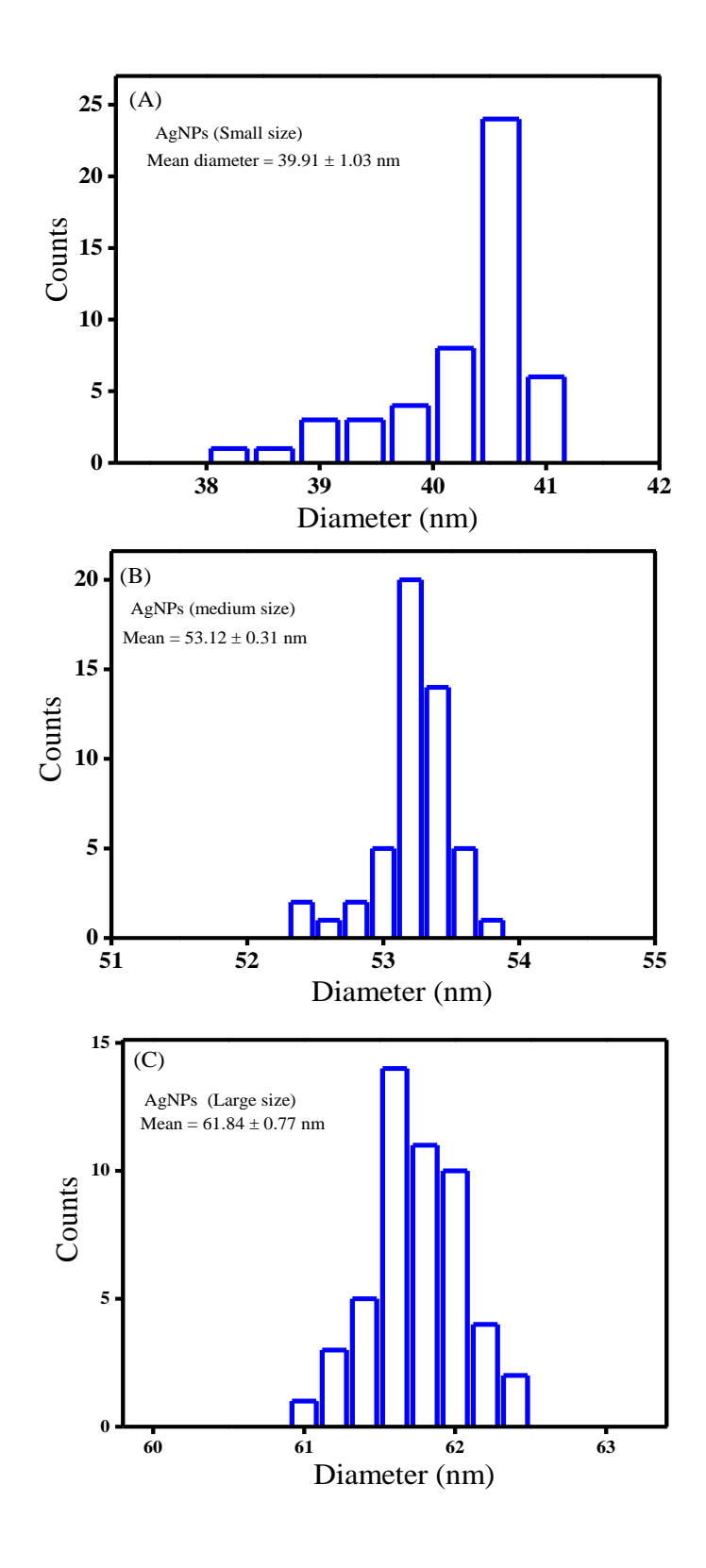


Figure 4. Size distribution histogram of (A) small, (B) medium and (C) large Ag NPs.

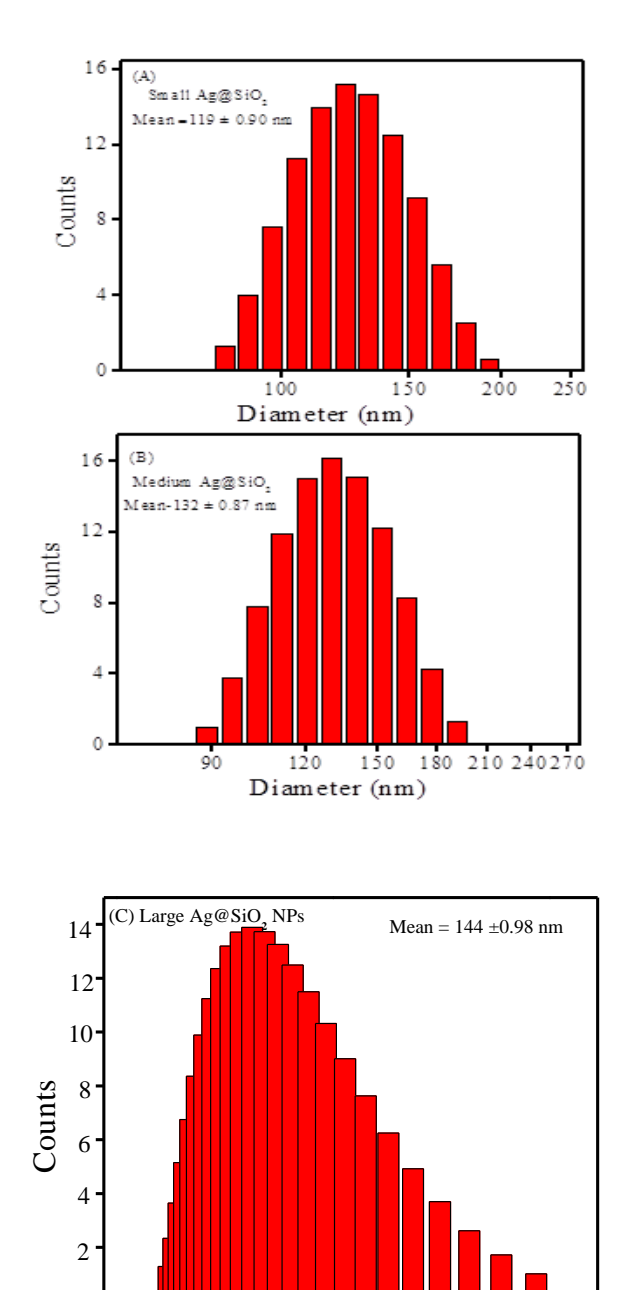


Figure 5. Size distribution histogram of (A) small, (B) medium (C) large $Ag@SiO_2$ NPs from DLS measurements.

Diameter (nm)

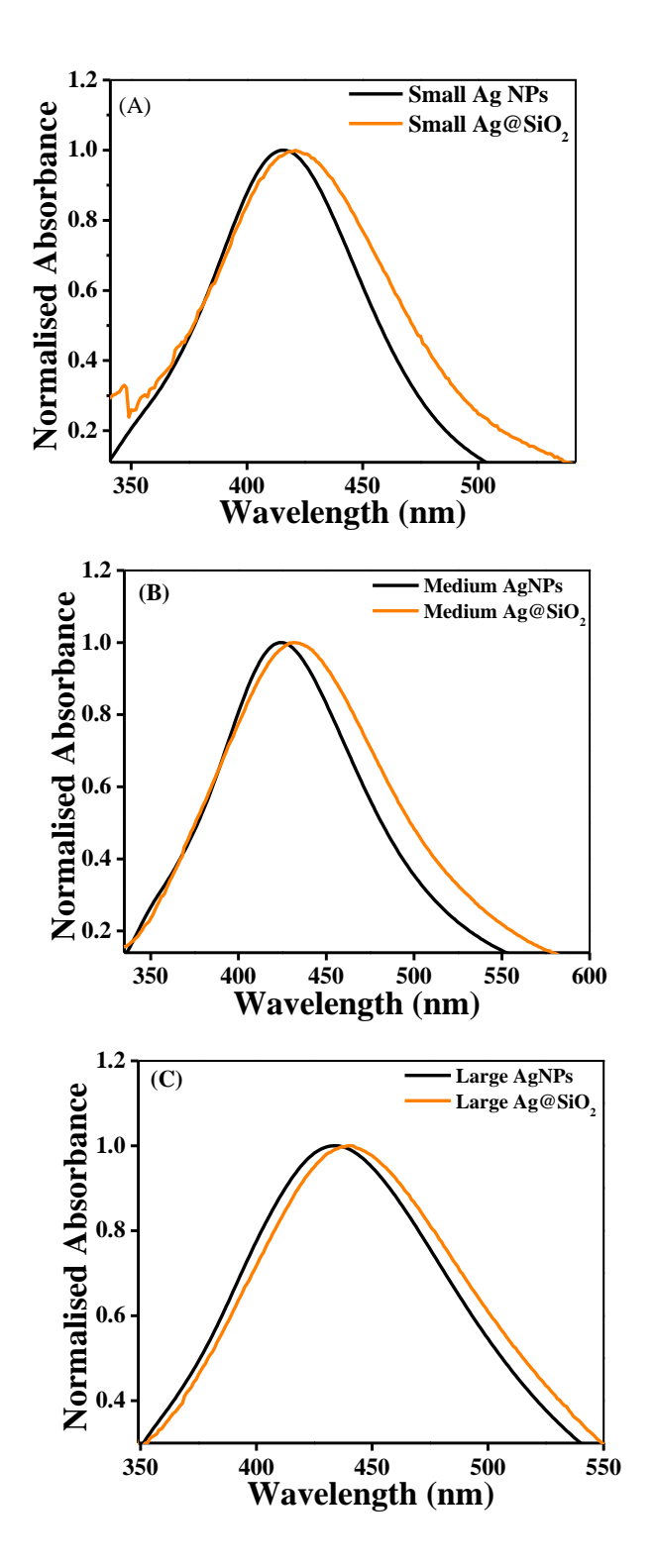


Figure 6. Changes in the LSPR of (A) small, (B) medium and (C) large silver nanoparticles when coated with a silica layer.

UV-visible spectroscopy was done for both bare and SiO₂-coated Ag NPs. The absorption spectra of small, medium and large Ag NPs show characteristic LSPR band centered at 415, 425, 435 nm for bare NPs and at 421, 432, 441 nm for coated NPs, respectively. The presence of silica shell on Ag NPs causes the red shift of the plasmon resonance band from 415 to 421 nm for small, 425 to 432nm for medium Ag NPs, 435 to 441nm for large Ag NPs because of a large refractive index of the silica shell and the decreased plasmon oscillation energy (Figure 6).

3.2 Characterization of carbon dot

Figure 7 shows the FTIR spectrum of CDs. The broad peak at 3420 cm⁻¹ is assigned to the stretching vibration of O–H and N–H moieties. The peak at 2925 cm⁻¹ is due to C–H stretching vibration. Two prominent peaks at 1690 and 1566 cm⁻¹ arise due to stretching and bending vibrations of CQO and N–H moieties respectively. Another noticeable peak at 1394 cm⁻¹ is assigned to the bending vibrations of C–H moieties.

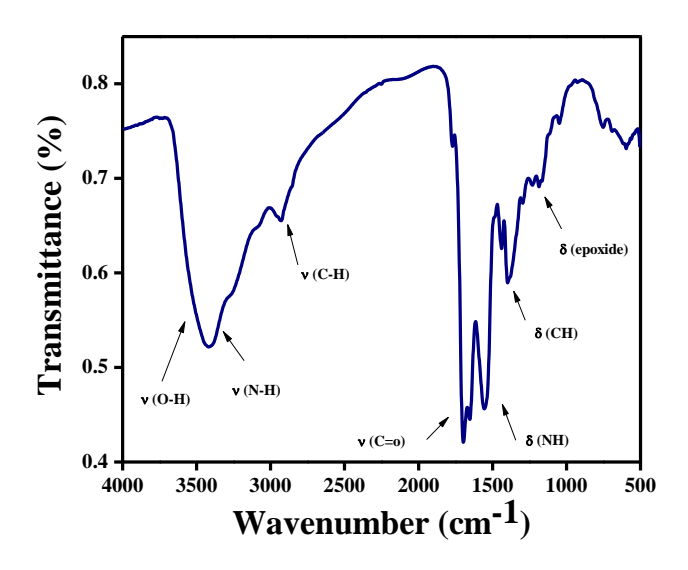


Figure 7. FTIR spectrum of synthesized CDs.

UV-Vis and fluorescence measurements were performed for 0.01 mg mL⁻¹ carbon dot. Absorption spectra of CDs show a narrow peak at 338 nm

wavelength. CDs show an intense PL band centered at 493 nm at an excitation wavelength 405 nm (Figure 8).

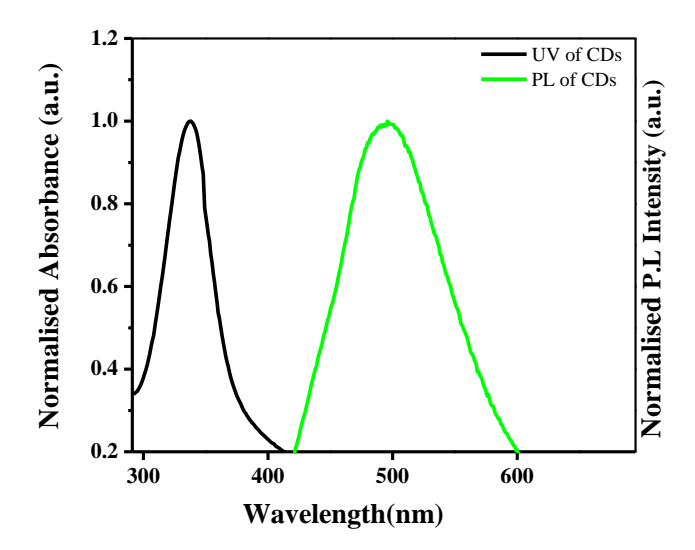


Figure 8. Absorbance spectrum (black line) and the normalized PL (λ_{ex} = 493 nm) spectrum (green line) of CDs.

3.3 Interaction of CDs and Ag NPs

UV-Vis spectroscopy was recorded for 0.01 mg mL⁻¹ CDs in the absence and presence of small, medium and large Ag NPs of 5, 10, 15 and 20 pM concentrations. The absorption spectrum of CDs a narrow absorption band at 338 nm. With the increase in the concentration of each small, medium and large Ag nanoparticles red shift was observed in the absorption maxima of CDs. These changes in absorption spectra indicate the possible interaction between CDs and three different sized silver nanoparticles (Figure 9).

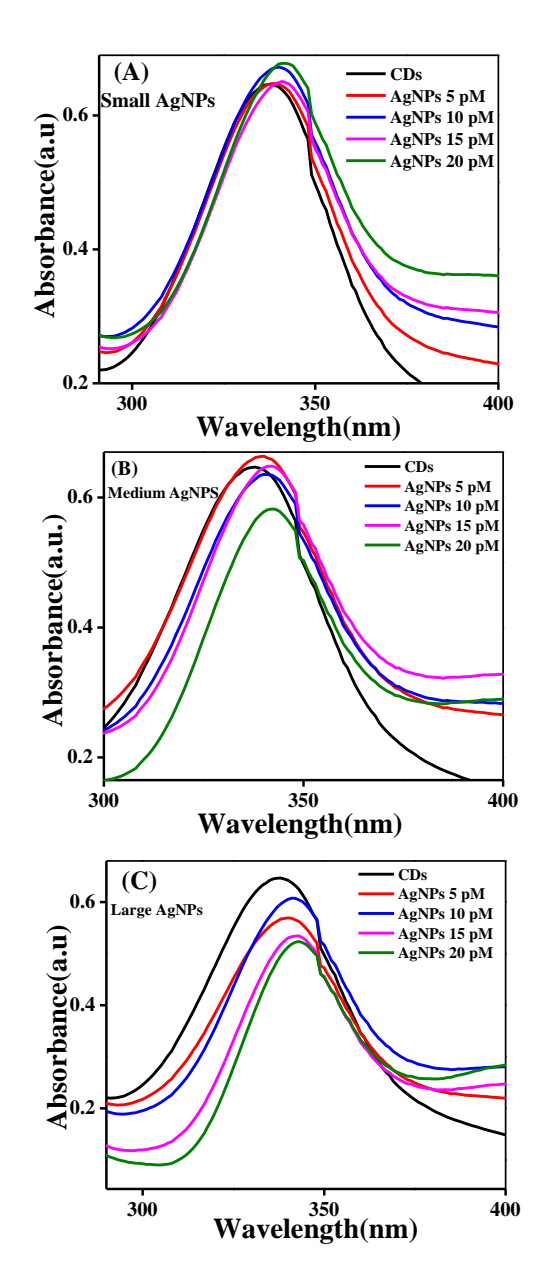


Figure 9. Absorption spectrum of CDs in the presence of (A) small, (B) medium and (C) large Ag NPs of 5,10,15 and 20 pM concentration.

3.4 Steady –State PL Quenching of CDs in the presence of Ag NPs and Ag@SiO₂ NPs.

CDs show an intense PL band centered at 493 nm at an excitation wavelength of 405 nm. The PL quantum yield of CDs decreases significantly with the successive addition of small, medium and large Ag

NPs. The decrease in quantum yield becomes more drastic when the coating was done on the three different sized Ag nanoparticles. From the control experiment with only trisodium citrate dihydrate ligand, it was seen that there is no changes in the absorption and PL spectra of CDs, which suggests that the surface of Ag NPs interacts with CDs instead of the surface citrate ligands

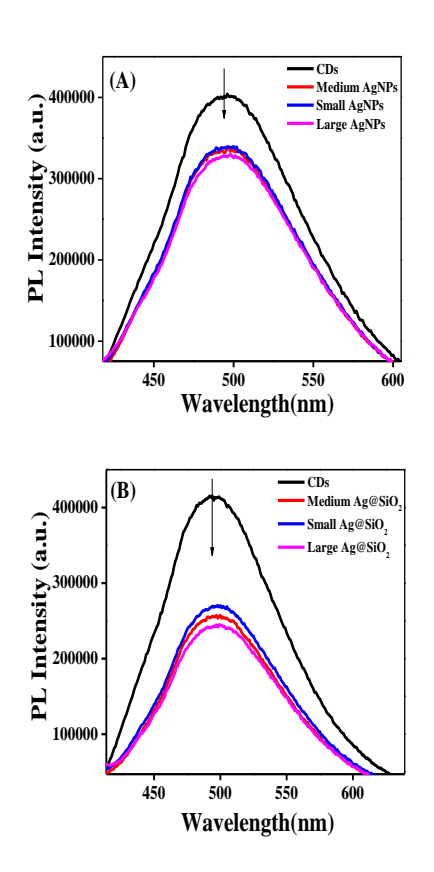


Figure 10. PL spectra of CDs in the presence of (A) 5 pM Ag NPs and (B) 5 pM Ag@SiO₂ NPs.

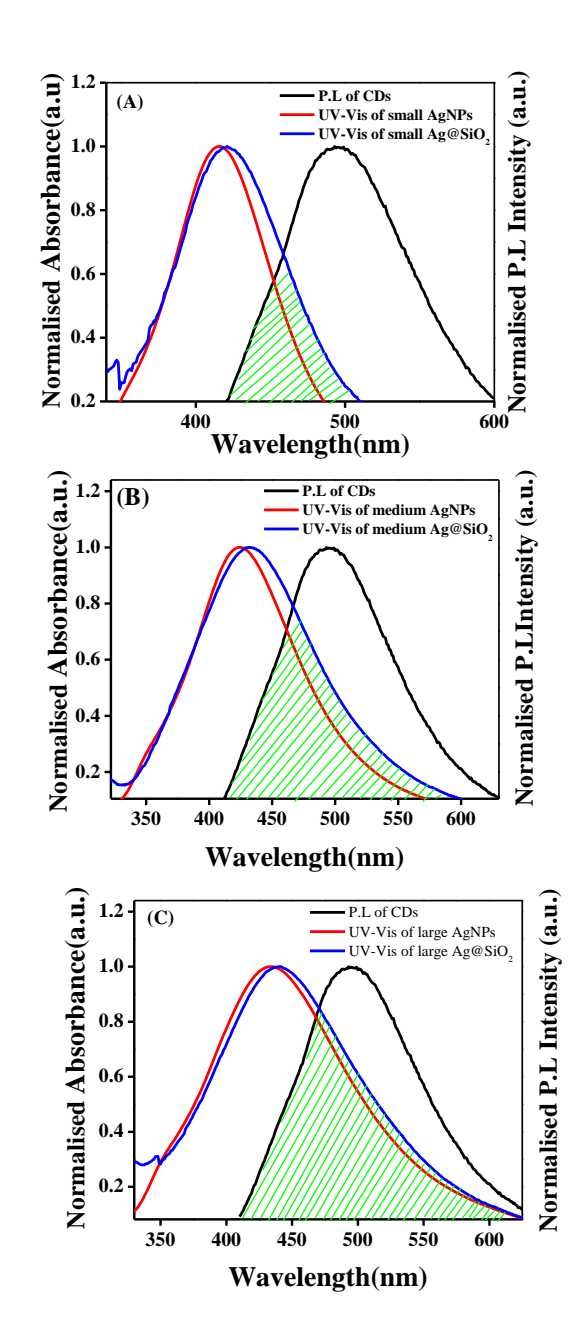


Figure 11. Normalized PL spectrum of CDs (black line) overlapped with the LSPR of uncoated (red line) and coated (blue line) (A) small (B) medium and (C) large silver nanoparticles.

The significant spectral overlap between the PL spectrum of CDs and LSPR band of Ag NPs signifies that the observed PL quenching of CDs in the presence of Ag NPs might be due to EET from CDs to Ag NPs.

Previously, it has been observed that noble-metal NP acts as an efficient fluorescence quencher for various organic dyes and quantum dots. [40,41,61-67] Figure 11, shows that spectral overlap increases with increase in the size of Ag NPs. Importantly, spectral overlap increases more appreciably when the coating was done on the three different sized nanoparticles. To establish the mechanism of EET from CDs to Ag NPs, we performed PL decay measurements.

3.5 Time-Resolve PL Quenching of CDs in the presence of Ag NPs

Figure 12. Shows the PL decay traces (λ_{em} = 493 nm) of CDs in the absence and presence of (A) uncoated Ag NPs and (B) SiO₂ coated Ag NPs. All of the decays were fitted with a three exponential decay function.

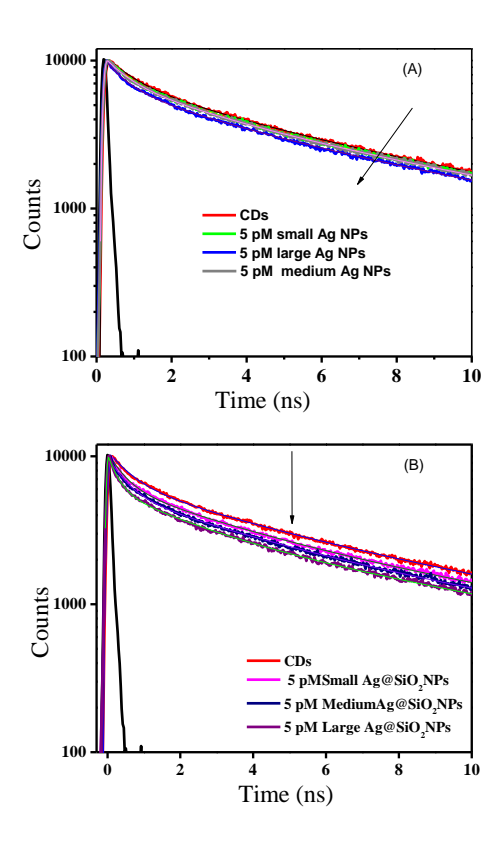


Figure 12. PL decay traces (λ_{ex} = 405 nm) of CDs in the absence and presence of (A) uncoated Ag NPs and (B) SiO₂-coated Ag NPs at different diameters.

The average PL lifetime of CDs is 4 ns with lifetime components of 2 (35%), 7.3 (43%), and 0.45 ns (22%), which is very close to the previously reported value. The addition of 5 pM small Ag NPs results in significant changes in the decay trace of CDs and the average PL lifetime decreases from 4 to 3.74 ns with lifetime components of 3.13 (37%), 9.31 (26%), and 0.45 ns (37%). The addition of 5 pM SiO₂ coated small Ag NPs results in significant decrease in the decay trace of CDs than the uncoated one and the average PL lifetime decreases from 4 to 2.5 ns with lifetime components of 2.54 (26%), 8.82 (19%), and 0.226 ns (55%) (Table1).

Table 1.PL Decay parameters of CDs, CDs with uncoated and coated small Ag NPs.

System	τ_1/ns	a_1	τ ₂ /ns	a_2	τ ₃ /ns	a ₃	<t></t>	χ^2
CDs	2.0	0.35	7.3	0.43	0.45	0.22	4	1.14
Small Ag NPs	3.13	0.37	9.31	0.26	0.45	0.37	3.74	1.2
Small Ag@SiO ₂	2.54	0.26	8.82	0.19	0.22	0.55	2.44	1.1

The addition of medium Ag NPs results in more significant changes in the decay trace of CDs as compared to the small Ag NPs and the average PL lifetime decreases from 4 to 3.42 ns with lifetime components of 0.28 (33%), 2.25 (35%), and 7.92 ns (32%). The addition of 5 pM SiO₂ coated medium Ag NPs results in drastic reduction in the decay trace of CDs than the uncoated one and the average PL life time decreases from 4 to 2.09 ns with lifetime components of 0.17 (59%), 2.16 (22%), and 0.19 ns (19%) (Table 2).

Table 2.PL Decay parameters of CDs and CDs with uncoated and coated medium Ag NPs.

System	τ_1/ns	a_1	τ ₂ /ns	a_2	τ ₃ /ns	a_3	<t> ns</t>	χ^2
CDs	2.0	0.35	7.3	0.43	0.45	0.22	4.0	1.1
Medium Ag NPs	0.28	0.33	2.25	0.35	7.92	0.32	3.42	1.2
Small Ag@SiO ₂	0.17	0.59	2.16	0.22	7.89	0.16	2.09	1.3

The addition of large uncoated Ag NPs results in appreciable changes in the decay trace of CDs than that of small and medium size uncoated Ag NPs and the average PL lifetime decreases from 4 to 2.35 ns with lifetime components of 0.35 (42%), 2.83 (33%), and 8.82 ns (20%). The addition of 5 pM SiO₂ coated large Ag NPs results in the substantial decrease in the PL decay trace of CDs than that of small and medium size coated Ag NPs. Here, the average PL life time decreases from 4 to 2.09 with lifetime components of 0.13 (75%), 2.13 (15%), and 8.19 ns (11%) (Table 3).

Table 3.PL Decay parameters of CDs and CDs with uncoated and coated large Ag NPs

System	τ_1/ns	a_1	τ ₂ /ns	a_2	τ ₃ /ns	a_3	<t></t>	χ^2
CDs	2.0	0.35	7.3	0.43	0.45	0.22	4.0	1.4
Large Ag NPs	0.35	0.42	2.83	0.33	8.82	0.20	2.35	1.28
Large Ag@SiO ₂	0.13	0.75	2.13	0.15	8.19	0.11	1.33	1.4

It is well known that metal NPs influence the intrinsic radiative and nonradiative decay rates of nearby fluorophores. [33, 41-42, 60, 61, 63, 64, 67] The shortened PL lifetime of CDs indicates that either the radiative or

nonradiative decay rate is increased in the presence of uncoated and coated Ag NPs .We have estimated the radiative and nonradiative decay rates of CDs in the presence of Ag NPs according to the following equation

$$k_{\rm r} = \frac{\Phi_{\rm D}}{\tau} \tag{3}$$

$$k_{\rm nr} = \left(\frac{1 - \Phi_{\rm D}}{\tau}\right) \tag{4}$$

Where k_r and k_{nr} are the radiative and nonradiative decay rates, respectively. ϕ_D is the quantum yield and τ is the average lifetime of the donor. All of the estimated parameters are listed in Table 4, 5, 6.

Table 4. Estimated Quantum Yields, Average Lifetime, Radiative Rates, Nonradiative Rates, Energy Transfer Rates, and Efficiency of Energy Transfer of CDs in the Absence and Presence of uncoated and coated small Ag NPs.

System	ϕ_{D}	τ (ns)	kr (s ⁻¹)	$k_{nr}(s^{-1})$	k_{ET} (S^{-1})	ϕ_{ET}
CDs	0.602	4	0.15×10^9	0.099×10^9		
Small Ag NPs	0.51	3.7	0.14×10 ⁹	0.132×10 ⁹	0.02 ×10 ⁹	0.07
Small Ag@SiO ₂	0.39	2.4	0.156×10 ⁹	0.249×10 ⁹	0.27 ×10 ⁹	0.39

Table 5.Estimated Quantum Yields, Average Lifetime, Radiative Rates, Nonradiative Rates, Energy Transfer Rates, and Efficiency of Energy

Transfer of CDs in the Absence and Presence of uncoated and coated medium Ag NPs.

System	ϕ_{D}	τ (ns)	kr (s ⁻¹)	$k_{nr}(s^{-1})$	$k_{ET}(s^{-1})$	фет
CDs	0.602	4	0.15×10^9	0.099×10^9		
Medium Ag NPs	0.485	3.42	0.142 ×10 ⁹	0.15×10 ⁹	0.05 ×10 ⁹	0.14
Medium Ag@SiO ₂	0.37	2.09	0.16 ×10 ⁹	0.3 ×10 ⁹	0.44 ×10 ⁹	0.48

Table 6. Estimated Quantum Yields, Average Lifetime, Radiative Rates, Nonradiative Rates, Energy Transfer Rates, and Efficiency of Energy Transfer of CDs in the Absence and Presence of uncoated and coated large AgNPs.

System	ϕ_{D}	τ (ns)	$k_r(s^{-1})$	$k_{nr}(s^{-1})$	$k_{ET}(s^{-1})$	фет
CDs	0.602	4	0.15×10^9	0.099×10^9		
Large Ag NPs	0.38	2.35	0.16×10 ⁹	0.27	0.31 ×10 ⁹	0.42
Large Ag@SiO ₂	0.223	1.33	0.16 ×10 ⁹	0.58	1.2×10 ⁹	0.61

It is evident from Table 4, 5, 6 that the nonradiative decay rate of CDs increases in the presence of uncoated Ag NPs when its size increases. The nonradiative decay rate of CDs increases appreciably due to the coating of SiO₂ on Ag NPs at three different thicknesses. Importantly, no appreciable change has been observed in the radiative decay rate of CDs upon the addition of uncoated and SiO₂ coated Ag NPs. Hence, the observed shortening of PL lifetime of CDs in the presence of uncoated and coated is due to the increased nonradiative decay rate rather than radiative decay rate. This increase in nonradiative decay rate in the presence of Ag NPs

can be explained by considering the nonradiative EET from CDs to Ag NPs.

We have measured the efficiency (Q_{Eff}) of this nonradiative EET process from the PL lifetimes of CDs in the absence and presence of uncoated and coated Ag NPs using the following equation

$$Q_{\rm Eff} = 1 - \frac{\tau_{\rm D-A}}{\tau_{\rm D}} \tag{5}$$

Where τ_{D-A} and τ_D are the excited state lifetimes of CDs in the presence and absence of Ag NPs respectively. It is evident from Table (4, 5, and 6) that the efficiency of EET from CDs increases significantly from 7 to 39, 14 to 48 and 41 to 61% when the coating was done on small, medium and large size Ag NPs respectively.

3.6. Mechanism of EET from CDs to Ag NPs.

To establish the mechanism behind this EET from the CDs to the Ag NPs, we have compared the experimentally obtained EET efficiencies with the theoretical curves calculated from NSET theory for the CDs-Ag NPs system. Persson's NSET theory is based on the collective interactions of all dipoles in a thin film near the metal surface and results in a 1/d

coupling instead of the conventional 1/d³ coupling. ^[68] According to the NSET mechanism, the rate of EET can be expressed as

$$k_{\text{NSET}} = \frac{1}{\tau_{\text{D}}} \left(\frac{d_0}{d}\right)^4 \tag{6}$$

Where τ_D is the excited-state lifetime of the donor in the absence of a acceptor, d is the distance between the donor and surface of the acceptor, and d_0 is the separation distance at which the energy transfer efficiency is 50%. The distance d_0 can be calculated by using the following equation

$$d_0 = \left(\frac{0.225\Phi_{\rm D}c^3}{\omega_{\rm D}^2\omega_{\rm F}k_{\rm F}}\right)^{1/4} \tag{7}$$

Where ϕ_D is the quantum yield of the donor, c is the velocity of light, ω_D is the angular frequency of the donor electronic transition, ω_F is the Fermi frequency, and k_F is the Fermi wave vector of the metal. For the present system, the d_0 value is calculated using $\phi_D = 0.602$, $c = 3 \times 10^{10}$ cm s⁻¹, $\omega_D = 5.57 \times 10^{15}$ s⁻¹, $\omega_F = 8.3 \times 10^{15}$ s⁻¹, and $k_F = 1.2 \times 10^8$ cm⁻¹. [69] The calculated d_0 for the CDs-Ag NP's system is 7.1 nm. Similarly, the Förster distance R_0 can be expressed as:

$$R_0 = [(8.8 \times 10^{-25})(\kappa^2 n^{-4} \Phi_D J(\lambda))]^{1/6}$$
 (8)

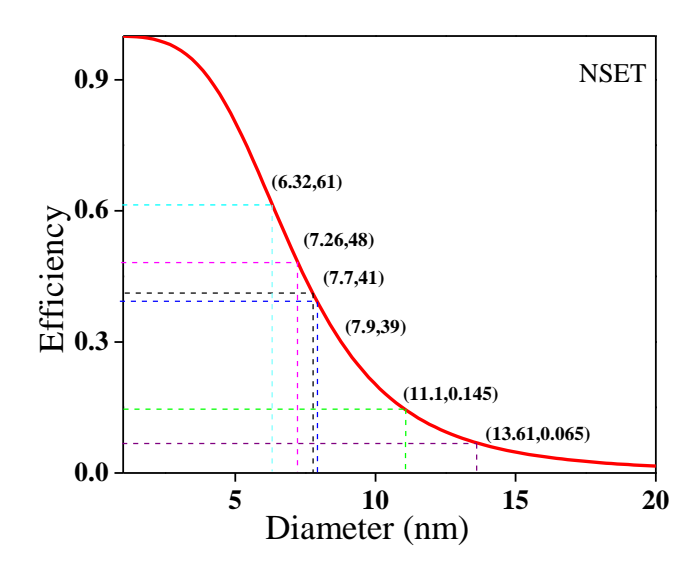
Where K^2 is the orientation factor of the transition dipoles of the donor and the acceptor, ϕ_D is the quantum yield of the donor, η is the refractive index of the medium, and $J(\lambda)$ is the overlap integral between the donor emission and the acceptor absorption spectrum. For the present CDs-Ag NP's system, the calculated overlap integral is $2.4\times10^{-8}M^{-1}$ cm³, and the estimated R_0 is 37.2 nm. Here it is important to mention that for an ideal FRET pair the typical Förster distance is in the range of 20-60 Å. [70, 71] Hence, for the present system the significantly higher value of R_0 that is

beyond the detection limit of FRET signifies that the present EET from CDs to Ag NPs does not follow the conventional FRET process. On the

basis of the estimated values of d_0 and R_0 , we have calculated the theoretical quenching efficiency as a function of distance according to the following equation

$$\Phi_{\rm ET} = \frac{1}{1 + \left(\frac{d}{d_0}\right)^n} \tag{9}$$

Where ϕ_{ET} is the energy transfer efficiency and d is the separation distance between CDs and Ag NPs. n is a factor that depends on the mechanism of energy transfer and has a value of either 6 or 4 for the FRET and NSET model, respectively. In the case of FRET, d_0 is equal to R_0 . Figure 13 Shows the theoretical plots of the quenching efficiency against the separation distance based on the NSET theory.



Figur13. Correlation between experimentally obtained EET efficiencies for the CDs-Ag NP's system with the theoretical curves generated from NSET (red line).

Experimentally obtained quenching efficiencies in the presence of uncoated and coated Ag NPs are shown on the Y axis of Figure 13. The estimated separation distance between CDs and the surface of uncoated small, medium and large Ag NPs are 13.61, 11.1, 7.7 nm respectively and the estimated separation distance between CDs and the surface of the coated small, medium and large Ag NPs are 7.7, 7.32, 6.32 nm respectively.

Chapter 4.

Conclusions and Future Prospects

4.1. Conclusions

In summary, the observed PL quenching of CDs in the presence of Ag NPs is mainly due to the EET from CDs to the surface of Ag NPs. The quenching in steady-state PL Intensity as well as in the excited-state lifetime of CDs in the presence of uncoated as well as SiO₂ coated Ag NPs arises due to the increased nonradiative decay rate, while the radiative decay rate remains almost constant. The experimentally estimated quenching efficiency from the lifetime data correlates well with the NSET mechanism rather than FRET mechanism. The drastic increment in the EET efficiency when coating was done on the three different size Ag NPs was observed due to the decreased distance between CDs and the surface of SiO₂ coated Ag NPs.

4.2. Scope of the future work

Recently, CDs becoming a very interesting fluorescence nanomaterial due to having its superior properties such as low cytotoxicity and good biocompatibility and it is implemented in bioimaging, biosensing, drug delivery, catalysis, and optronics etc. We know that excitation energy transfer in nanoscale donor-acceptor system has a large-scale implementation in bioimaging, bio sensing etc. Here in this report, we have modulated the energy transfer efficiency of CDs varying the size of Ag NPs. In future, my plan is to modulate the luminescence properties of CDs by varying the shape of Ag NPs.

References

- [1] Yin D., Wang C., Ouyang J., Zhang X., Zheng Jiao, Feng Yi ., Song K., Liu B., Cao X., Zhang Lu., Han Y., Wu M. (2014), Synthesis of a Novel Core-Shell Nanocomposite Ag@SiO₂@Lu₂O₃:Gd/Yb/Er for Large Enhancing Upconversion Luminescence and Bioimaging, *ACS Appl. Mater, Interfaces*, **6**, 18480–18488.
- [2] Rogach A. L., Gaponik N., J Lupton. M., Bertoni C., Gallardo D. E., Dunn S., Pira N. L., Paderi M., Repetto P., Romanov S. G., Dwyer C. O., Torres C. M. S. (2008), Eychmller Light-Emitting Diodes with Semiconductor Nanocrystals, *Angew. Chem. Int. Ed.*, **47**, 6538 6549.
- [3] Li X., Choy W. C. H., Huo L., Xie F., Sha W. E. I., Ding B., Guo X., Li Y., Hou J., You J., Yang Y. (2012), Dual Plasmonic Nanostructures for High-Performance Inverted Organic Solar Cells, *Adv. Mater.*, **24**, 3046 52.
- [4] Kim J., Koh J. K., Kim B., Kim J. H., Kim E. (2012), Nanopatterning of Mesoporous Inorganic Oxide Films for Efficient Light Harvesting of Dye-Sensitized Solar Cells, *Angew. Chem., Int. Ed.*, **51**, 6864-9.
- [5] Zheng Z., Huang B., Qin X., Zhang X., Dai Y. (2011), Facile *in Situ* Synthesis of Visible-Light Plasmonic Photocatalysts M@TiO₂ (M = Au, Pt, Ag) and Evaluation of Their Photocatalytic Oxidation of Benzene to Phenol, *J. Mater. Chem.*, **21**, 9079.
- [6] Zhou L., Ding F., Chen H., Ding W., Zhang W., Chou S. Y. (2012), Enhancement of Immunoassay's Fluorescence and Detection Sensitivity Using Three-Dimensional Plasmonic Nano-Antenna-Dots Array, *Anal. Chem.*, **84**, 4489–4495.
- [7] Taylor A. B., Kim J., Chon J. W. M. (2012), Detuned Surface Plasmon Resonance Scattering of Gold Nanorods for Continuous Wave Multilayered Optical Recording and Readout, *Opt. Express*, **20**, 5069.
- [8] Nolan E.M., Lippard S.J. (2008), Tools and Tactics for the Optical Detection of Mercuric Ion., *Chem.Rev.*, **108**, 3443-3480.

- [9] Rasnik I., McKinney S.A., Ha T. (2005), Surface and Orientations: Much to FRET about ? *Acc Chem.Res.*, **38**, 542-548.
- [10] Brown M.D., Auteewong T., Kumar R.S.S., D Innocenzo V., Petozza A., Lee M.M., Weinsner U., Snaith H.J, (2011), Plasmonic Dye-Sensitized Solar Cells Using Core-Shell Metal–Insulator Nanoparticles, *Nano.Lett.*, **11**, 438-445.
- [11] Wang Y., Xie X., Goodson T. (2005), Enhanced Third-Order Non-Linear Optical Properties in Dendrimer-Metal Nanocomposites, *Nano Lett.*, **5**, 2379-2348.
- [12] L u S., Liinger Z., Asano T., Harris D., Barwicz T., Guha S., Madhukar A. (2009), Photocurrent Induced by Nonradiative Energy Transfer From Nanocrystal Quantum Dots to Adjacent Silicon Nanowire Conducting Channels: Towards a New Solar Cell Paradigm, *Nano Lett.* **9**, 4548-4552.
- [13] Scholes G. D. (2003), Long-Range Resonance Energy Transfer in Molecular Systems, *Annu. Rev. Phys. Chem.*, **54**, 57–58.
- [14] Beljonne D., Curutchet C., Scholes G. D., Silbey R. J. (2009), Beyond Förster Resonance Energy Transfer in Biological and Nanoscale Systems, *J. Phys. Chem. B*, **113**, 6583–6599.
- [15] Wong K. F., Bagchi B., Rossky P. J. (2004), Distance and Orientation Dependence of Excitation Transfer Rates in Conjugated Systems: Beyond the Förster Theory, *J. Phys. Chem. A*, **108**, 5752–5763.
- [16] Rao V. G., Mandal S., Ghosh S., Banerjee C., Sarkar N. (2012), Study of Fluorescence Resonance Energy Transfer in Zwitterionic Micelles: Ionic-Liquid-Induced Changes in FRET Parameters, *J. Phys. Chem. B*, **116**, 12021–12029.
- [17] Gupta S., Adhikari A., Mandal A. K., Bhattacharyya K., Ramamurthy V. (2011), Ultrafast Singlet-Singlet Energy Transfer Between an Acceptor Electrostatically Attached to the Walls of an Organic Capsule and the Enclosed Donor, *J. Phys. Chem. C*, **115**, 9593–9600.

- [18] Bhattacharyya S., Barman M. K., Baidya A., Patra A. (2014), Singlet Oxygen Generation from Polymer Nanoparticles-Photosensitizer Conjugates Using FRET Cascade, *J. Phys. Chem. C*, **118**, 9733–9740.
- [19] Clapp A. R., Medintz I. L., Mauro J. M., Fisher B. R., Bawendi M. G., Mattoussi H. J. (2004), Fluorescence Resonance Energy Transfer Between Quantum Dot Donors and Dye-Labeled Protein Acceptors, *Am. Chem. Soc.*, **126**, 301–310.
- [20] Medintz I. L., Clapp A. R., Mattoussi H., Goldman E. R., Fisher B., Mauro J. M.(2003), Self-Assembled Nanoscale Biosensors Based on Quantum Dot FRET Donors, *Nat. Mater*, **2**, 630–638.
- [21] Naiki H., Masuhara A., Masuo S., Onodera T., Kasai H., Oikawa H. (2013), Highly Controlled Plasmonic Emission Enhancement from Metal-Semiconductor Quantum Dot Complex Nanostructures, *J. Phys. Chem. C*, **117**, 2455–2459.
- [22] Li M., Cushing S. K., Wang Q., Shi X., Hornak L. A., Hong Z., Wu N. (2011), Size-Dependent Energy Transfer between CdSe/ZnS Quantum Dots and Gold Nanoparticles, *J. Phys. Chem. Lett.*, **2**, 2125–2129.
- [23] Sen T., Patra A. (2012), Recent Advances in Energy Transfer Processes in Gold-Nanoparticle-Based Assemblies, *J. Phys. Chem. C*, **116**, 17307–17317.
- [24] Quach, A. D., Crivat, G., Tarr, M. A., Rosenzweig, Z. (2011), Gold Nanoparticle-Quantum Dot-Polystyrene Microspheres as Fluorescence Resonance Energy Transfer Probes for Bioassays, *J. Am. Chem. Soc.*, **133**, 2028–2030.
- [25] Eustis S., EI-Sayed M. A. (2006), Why Gold Nanoparticles are More Precious than Pretty Gold: Noble Metal Surface Plasmon Resonance and its Enhancement of the Radiative and Nonradiative Properties of Nanocrystals of Different Shapes, *Chem. Soc. Rev.*, *35*, 209–217.
- [26] Link S., E.I.Sayed MA. (2003), Optical Properties and Ultrafast Dynamics of Metallic Nanocrystals, *Rev.*, *Phys. Chem.*, **54**, 331–366.

- [27] Nie S., Emory S. R. (1997), Probing Single Molecules and Single Nanoparticles by Surface-Enhanced Raman Scattering, *Science*, **275**, 1102–1106.
- [28] He L., Langlet M., Bouvier P., Calers C., Pradier C. M., Stambouli V. (2014), New Insights into Surface-Enhanced Raman Spectroscopy Label-Free Detection of DNA on Ag⁰/TiO₂ Substrate, *J. Phys. Chem. C*, **118**, 25658–25670.
- [29] Sánchez E. J., Novotny L., Xie X. S. (1999), Near-Field Fluorescence Microscopy Based on Two-Photon Excitation with Metal Tips, *Phys. Rev. Lett.*, **82**, 4014–4017.
- [30] Protasenko V. V., Gallagher A. C. (2004), Apertureless Near-Field Scanning Optical Microscopy of Single Molecules, *Nano Lett.*, **4**, 1329-1332.
- [31] Shimizu K. T., Woo W. K., Fisher B. R., Eisler H. J., Bawendi M. G. (2002), Surface-Enhanced Emission from Single Semiconductor Nanocrystals, *Phys. Rev. Lett.*, **89**, 117401.
- [32] Kühn S., Håkanson U., Rogobete L., Sandoghdar V. (2006), Enhancement of Single-Molecule Fluorescence Using a Gold Nanoparticle as an Optical Nanoantenna, *Phys. Rev. Lett.*, **97**, 017402.
- [33] Chen Y., Munechika K., Ginger D. S. (2007), Dependence of Fluorescence Intensity on the Spectral Overlap between Fluorophores and Plasmon Resonant Single Silver Nanoparticles, *Nano Lett.*, **7**, 690-696.
- [34] Munechika K., Chen Y., Tillack A. F., Kulkarni A. P., Plante I. J. L., Munro A. M., Ginger D. S. (2010), Spectral Control of Plasmonic Emission Enhancement from Quantum Dots near Single Silver Nanoprisms, *Nano Lett.*, **10**, 2598–2603.
- [35] Pan S. L., Wang Z. J., Rothberg L. J. (2006), Enhancement of Adsorbed Dye Monolayer Fluorescence by a Silver Nanoparticle Overlayer, *J. Phys. Chem. B*, **110**, 17383–17387.

- [36] Xie F., Baker M. S., Goldys E. M. (2006), Homogeneous Silver-Coated Nanoparticle Substrates for Enhanced Fluorescence Detection, *J. Phys. Chem. B*, **110**, 23085–23091.
- [37] Liu Y., Wu P. (2013), Meditating Metal Coenhanced Fluorescence and SERS Around Gold Nanoaggregates in Nanosphere as Bifunctional Biosensor for Multiple DNA Targets, *ACS Appl. Mater. Interfaces*, **5**, 5832–5844.
- [38] Prajapati R., Chatterjee S., Bhattacharya A., Mukherjee T. K. M.(2015), Surfactant-Induced Modulation of Nanometal Surface Energy Transfer from Silicon Quantum Dots to Silver Nanoparticles, *Phys. Chem. C.*, **119**, 13325–13334.
- [39] Naiki H., Masuhara A., Masuo, S., Onodera T., Kasai H., Oikawa H. (2013), Highly Controlled Plasmonic Emission Enhancement from Metal-Semiconductor Quantum Dot Complex Nanostructures, *J. Phys. Chem. C*, **117**, 2455-2459.
- [40] Munechika K., Chen Y., Tillack A. F., Kulkarni A. P., Plante I. J. L., Munro A. M., Ginger D. S. (2010), Spectral Control of Plasmonic Emission Enhancement from Quantum Dots near Single Silver Nanoprisms, *Nano Lett.*, **10**, 2598-2603.
- [41] Thomas K. G., Kamat P. V. (2000), Making Gold Nanoparticles Glow: Enhanced Emission from a Surface-Bound Fluoroprobe, *J. Am. Chem. Soc.*, **122**, 2655–2656.
- [42] Raghavendra U.P., Thipperudrappa J., Basanagouda M., Melavanki R.M. (2016), Influence of Silver Nanoparticles on Spectroscopic Properties of Biologically Active Iodinated 4-Aryl Oxymethyl Coumarin Dyes, *Journal of Luminescence*, **172**, 139-146.
- [43] Chance R. R., Prock A., Silbey R. (1978), Molecular Fluorescence and Energy Transfer Near Interfaces, *Adv. Chem. Phys.*, **37**, 1-65.
- [44] Sevilla M. and. Fuertes A. B. (2009), Chemical and Structural Properties of Carbonaceous Products Obtained by Hydrothermal Carbonization of Saccharides, *Chem.-Eur. J*, **15**, 4195–4203.

- [45] Dulkeith E., Ringler M., Klar T. A., Feldmann J., Muñoz Javier A., Parak W. J. (2005), Gold Nanoparticles Quench Fluorescence by Phase Induced Radiative Rate Suppression, *Nano Lett.*, **5**, 585–589.
- [46] Jennings T. L., Singh M. P., Strouse G. F. (2006), Fluorescent Lifetime Quenching near d =1.5 nm Gold Nanoparticles: Probing NSET Validity, *J. Am. Chem. Soc.*, **128**, 5462–5467.
- [47] Yun C. S., Javier A., Jennings T., Fisher M., Hira S., Peterson S., Hopkins B., Reich N. O., Strouse G. F. (2005), Nanometal Surface Energy Transfer in Optical Rulers, Breaking the FRET Barrier, *J. Am. Chem. Soc.*, **127**, 3115-3119.
- [48] Dulkeith E., Morteani, A. C., Niedereichholz T., Klar T. A., Feldmann J., Levi S. A., van Veggel F. C. J. M., Reinhoudt D. N., Möller M., Gittins D. I. (2002), Fluorescence Quenching of Dye Molecules near Gold Nanoparticles: Radiative and Nonradiative Effects, *Phys. Rev. Lett.*, **89**, 203002.
- [49] Li M., Cushing S. K., Wang Q., Shi X., Hornak L. A., Hong Z., Wu N. (2011), Size-Dependent Energy Transfer Between CdSe/ZnS Quantum Dots and Gold Nanoparticles, *J. Phys. Chem. Lett.*, **2**, 2125–2129.
- [50] Derfus A. M., Chan W. C. W., and Bhatia, S. N. (2004), Probing the Cytotoxicity of Semiconductor Quantum Dots, *Nano Lett.*, **4**, 11-18.
- [51] Kirchner C. Liedl T., S. Kuder., T. Pellegrino., A. M. Javier., H. E. Gaub., S. Sto Zele., N. Fertig and W. J. Parak. (2005), Cytotoxicity of Colloidal CdSe and CdSe/ZnS Nanoparticles, *Nano Lett.*, **5**, 331-338. 6473-6475.
- [52] S. Zhu., Q. Meng., L. Wang., J. Zhang., Y. Song., H. Jin., K. Zhang., H. Sun., H. Wang and B. Yang. (2013), Highly Photoluminescent Carbon Dots for Multicolor Patterning, Sensors, and Bioimaging, *Angew. Chem.*, *Int. Ed.*, **52**, 3953-3957.
- [53] C. Liu., P Zhang., F Tian., W Li., F Li and W. Liu. (2011), One-Step Synthesis of Surface Passivated Carbon Nano Dots by Microwave

- Assisted Pyrolysis for Enhanced Multicolor Photoluminescence and Bioimaging, *J. Mater. Chem.*, **21**, 13163-13167.
- [54] S. Sahu., B. Behera., T.K. Maiti and S. Mohapatra. (2012), Simple One-Step Synthesis of Highly Luminescent Carbon Dots from Orange Juice: Application as Excellent Bio-Imaging Agents, *Chem. Commun*, **48**, 8835–8837.
- [55] De B and Karak N., Sevilla M. and. Fuertes A. B. (2013), Chemical and Structural Properties of Carbonaceous Products Obtained by Hydrothermal Carbonization of Saccharides, *RSC Adv.*, **3**, 8286-8290.
- [56] Sun Y.-P., Zhou B., Lin Y., Wang W., Fernando K. A. S., Pathak P., Meziani M. J., Harruff B. A., Wang X., Wang H. F., Luo P. G., Yang H., Kose M. E., Chen B. L., Veca L. M. and Xie S.Y. (2006), Bandgap-Like Strong Fluorescence in Functionalized Carbon Nanoparticles, *J. Am. Chem. Soc.*, **128**, 7756–7757.
- [57] Bhattacharya A, Chatterjee S, Prajapati R, Mukherjee T. K. (2015), Size-Dependent Penetration of Carbon Dots Inside the Ferritin Nanocages: Evidence for the Quantum Confinement Effect in Carbon Dots, *Chem. Chem. Phys.*, 17, 12833.
- [57] Lee, P. C., Meisel D. (1982), Adsorption and Surface-Enhanced Raman of Dyes on Silver and Gold Sols, *J. Phys. Chem.*, **86**, 3391–3395.
- [58] Paramelle D., Sadovoy A., Gorelik S., Free P., Hobley J., Fernig D. G. (2014), A Rapid Method to Estimate the Concentration of Citrate Capped Silver Nanoparticles from UV-Visible Light Spectra, *Analyst*, **139**, 4855–4861.
- [59] Lu L., Qian Y., Wang L., Ma K., and Zhang Y. (2014), Metal-Enhanced Fluorescence-Based Core-Shell Ag@SiO₂ Nanoflares for Affinity Biosensing via Target Induced Structure Switching of Aptamer, *ACS Appl. Mater. Interfaces*, **6**, 1944-1950.
- [60] Munechika K., Chen Y., Tillack A. F., Kulkarni A. P., Plante I. J. L., Munro A. M., Ginger D. S. (2010), Spectral Control of Plasmonic

- Emission Enhancement from Quantum Dots near Single Silver Nanoprisms, *Nano Lett.*, **10**, 2598-2603.
- [61] Pan S. L., Wang Z. J., Rothberg L. J. (2006), Enhancement of Adsorbed Dye Monolayer Fluorescence by a Silver Nanoparticle Overlayer, *J. Phys. Chem. B.*, **110**, 17383-17387.
- [62] Kuhnke K., Becker R., Epple M., Kern K. (1997), C60 Exciton Quenching near Metal Surfaces, *Phys. Rev. Lett.*, **79**, 3246–3249.
- [63] Shimizu K. T., Woo W. K., Fisher B. R., Eisler H. J., Bawendi M. G. (2002), Surface-Enhanced Emission from Single Semiconductor Nanocrystals, *Phys. Rev. Lett.*, **89**, 117401.
- [64] Kühn S., Håkanson U., Rogobete L., Sandoghdar V. (2006), Enhancement of Single-Molecule Fluorescence Using a Gold Nanoparticle as an Optical Nanoantenna, *Phys. Rev. Lett.*, **97**, 017402.
- [65] Chen Y., Munechika K., Ginger D. S. (2007), Dependence of Fluorescence Intensity on the Spectral Overlap between Fluorophores and Plasmon Resonant Single Silver Nanoparticles, *Nano Lett.*, **7**, 690–696...
- [67] Xie F., Baker M. S., Goldys E. M. (2006), Homogeneous Silver-Coated Nanoparticle Substrates for Enhanced Fluorescence Detection, *J. Phys. Chem. B*, **110**, 23085-23091.
- [68] Persson B. N. J., Lang N. D. (1982), Electron-Hole-Pair Quenching of Excited States near a Metal, *Phys. Rev. B*, **26**, 5409–5415.
- [69] Saraswat S., Desireddy A., Zheng D., Guo L., Lu H. P., Bigioni T. P., Isailovic D. (2011), Energy Transfer from Fluorescent Proteins to Metal Nanoparticles, *J. Phys. Chem. C*, **115**, 17587–17593
- [70] Lakowicz, J. R., (1999), Principles of Fluorescence Spectroscopy, 2nd ed. Academic Press: New York.
- [71] Mandal S., Ghatak C., Rao V. G., Ghosh S., Sarkar N. (2012), Pluronic Micellar Aggregates Loaded with Gold Nanoparticles (Au NPs) and Fluorescent Dyes: A Study of Controlled Nanometal Surface Energy Transfer, *J. Phys. Chem. C*, **116**, 5585–5597.